© American Society for Mass Spectrometry, 2013

J. Am. Soc. Mass Spectrom. (2013)
DOI: 10.1007/s13361-013-0579-z

RESEARCH ARTICLE

A Database of Alkaline-Earth-Coordinated Peptide Cross Sections: Insight into General Aspects of Structure

Jonathan M. Dilger,[1] Stephen J. Valentine,[2] Matthew S. Glover,[1] David E. Clemmer[1]

[1]Department of Chemistry, Indiana University, Bloomington, IN 47405, USA
[2]Department of Chemistry, West Virginia University, Morgantown, WV 26506, USA

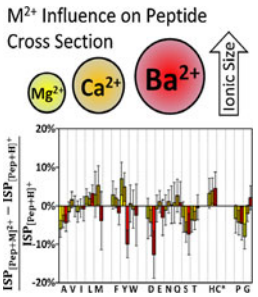

Abstract. A database of 1470 collision cross sections (666 doubly- and 804 triply-charged) of alkaline-earth-coordinated tryptic peptide ions [where the cation (M^{2+}) correspond to Mg^{2+}, Ca^{2+}, or Ba^{2+}] is presented. The utility of such an extensive set of measurements is illustrated by extraction of general properties of M^{2+}-coordinated peptide structures. Specifically, we derive sets of intrinsic size parameters (ISPs) for individual amino acid residues for M^{2+}-coordinated peptides. Comparison of these parameters with existing ISPs for protonated peptides suggests that M^{2+} binding occurs primarily through interactions with specific polar aliphatic residues (Asp, Ser, and Thr) and the peptide backbone. A comparison of binding interactions for these alkaline-earth metals with interactions reported previously for alkali metals is provided. Finally, we describe a new analysis in which ISPs are used as probes for assessing peptide structure based on amino acid composition.

Key words: Ion mobility spectrometry, Intrinsic amino acid size parameters, Peptide ion structure

Received: 3 September 2012/Revised: 14 December 2012/Accepted: 20 December 2012

Introduction

Metal-containing protein conformations arise from a balance of many interactions, including those that are intrinsic to the polypeptide chain and those that are induced upon binding of a metal cofactor [1–3]. In some cases, it appears that the protein sequence has evolved to contain a metal. In such a case, the protein retains its structure, regardless of the presence of the metal in the binding site. In other cases, the interactions leading to metal binding may have a substantial influence on the entire protein conformation, even regions that are distal to the metal. Because so many proteins require metal ions in order to adopt functional structures, and because so many different types of metals (12 "life metals" are particularly relevant for vital activity in biological systems) [3] are used, it is of interest to develop a fundamental understanding of metal–polypeptide interactions [4–24].

In the work presented here, we report a relatively large database of metal ion-containing peptide collision cross sections for the alkaline-earth series Mg^{2+}, Ca^{2+}, and Ba^{2+}. The cross section of an ion is a measure of its overall shape and, thus, is related to its structure. These measurements are carried out in the gas phase and, thus, provide a direct look at the intramolecular interactions of metal-containing peptides in the absence of effects associated with solvation. From the data that are obtained, we are able to determine likely binding interactions.

The present work is possible because of the advent of soft ionization techniques developed for mass spectrometry (MS) [25]. MS measurements provide information about metal–protein stoichiometry as well as insight into metal coordination sites [26–31] even when only minute quantities of sample are available. Recently, we used ion mobility-mass spectrometry (IMS-MS) techniques to generate a large database of 1772 peptide ion collision cross sections of which 954 entries incorporated the alkali cations Li^+, Na^+, K^+, and Cs^+ [32]. From these data, it was possible to determine that alkali metal cations are primarily solvated by certain polar residues (specifically Asp, Glu, Asn, Gln, His, and carboxyamidomethylated Cys). In this paper, we expand these measurements to study the influence of alkaline-earth metal cations on peptide ion structure. Such a large dataset makes it possible to obtain insight about general trends in peptide ion structure upon binding to alkaline-earth cations. Correlations can be drawn between these relative sizes and the amino acid composition of the peptide ion with the derivation of intrinsic size parameters (ISPs) [33–36]. These ISPs suggest which amino acids are generally associated with binding each metal.

Electronic supplementary material The online version of this article (doi:10.1007/s13361-013-0579-z) contains supplementary material, which is available to authorized users.

Correspondence to: David E. Clemmer; *e-mail:* Clemmer@Indiana.edu

Published online: 20 March 2013

Another important aspect of ISPs is that they provide a means for predicting collision cross sections [33, 36]. Such predictions can be used to refine assignments of unknown sequences that are generated by MS/MS analyses combined with database searching methodologies [37]. Below, we demonstrate a new use of this approach by applying the ISPs derived from the $[Pep + M]^{2+}$ peptide ions to predict cross sections for the observed $[Pep + M + H]^{3+}$ peptide ions. The idea that some sequences containing an additional proton can be predicted from ISP values derived from sequences containing only the metal ion suggests that the parameters may be identifying elements of structure that are imposed by the metal (i.e., the similar metal binding interactions are defining the structure with and without an additional proton).

Experimental

Instrumentation

General theoretical and experimental aspects of IMS techniques are discussed elsewhere [38–44]. Briefly, for the measurements reported here, nested IMS-MS measurements were recorded using a home-built instrument [45–47]. Solutions of tryptic peptides are electrosprayed using a Nanomate autosampler (Advion Biosciences, Inc., Ithaca, NY, USA). Sample ions are electrosprayed directly into a Smith-geometry hour-glass ion funnel that is operated as a trap [48, 49]. Ions accumulate in the ion funnel trap, and an electrostatic ion gate is periodically lowered in order to release pulses of ions into a 1.8 m drift tube. Diffusing ions are guided through the drift tube containing ~3 Torr of He buffer gas (300 K) under the influence of a uniform electric field (~10 $V \cdot cm^{-1}$). Ion packets are radially focused with two ion funnels (one in the middle of the drift tube and one as the ions exit the drift tube). Upon exiting the drift tube, mobility-separated ions are extracted into a home built orthogonal geometry reflectron time-of-flight mass spectrometer. Because flight times in the mass analysis region are much shorter than drift times in the ion mobility region, it is possible to record data in a nested fashion, as described previously [50].

Sample Preparation of Mixtures of Peptide Ions

The protocol for the tryptic digestion of known protein and protein subunits to produce large mixtures of peptides is described elsewhere [32]. Briefly, for the samples that were analyzed here, tryptic peptide solutions were suspended in a 50:50 acetonitrile:water solution at a concentration of ~0.1 $mg \cdot mL^{-1}$. Acid was omitted to reduce competition of free protons in solution with the alkaline-earth metal cations. Separate solutions containing each alkaline-earth cation with the addition of metal acetate (Aldrich or Sigma, St. Louis, MO, USA) at a concentration of ~0.5 mM were prepared for introduction into the IMS-MS instrument by electrospray ionization (ESI). Competition of the metal cations and protons leads to a distribution of charge carriers, as described below.

Peptide Ion Assignments

Distributions of peptide ions (either protonated or metalated by Mg^{2+}, Ca^{2+}, or Ba^{2+}) were produced by ESI and introduced into the source region of the IMS-MS instrument, where nested mobility and mass information was collected for 5 min per sample. Software (developed in house) was used to pick the positions of peaks in the two dimensional datasets. This resulted in lists of experimental *m/z* values for each specific protein digestion that could be compared with expected values (i.e., theoretically calculated) generated by the ExPASy Proteomics Server PeptideMass [51] online tool. In the present analysis, we considered peptides containing up to two missed cleavages. A peak-picking tolerance of 0.25 *m/z* with a five-count intensity threshold was set for locating all peaks of interest above the noise threshold. Drift time distributions for each picked peak were obtained at the monoisotopic mass by integrating all *m/z* bins (across a range corresponding to ±0.25 *m/z*) at each drift time. Specific drift times were recorded for peak maxima of prominent features within the drift time distribution. All recorded peak maxima were visually verified against the nested IMS-MS datasets for verification of expected charge state or possible interfering peaks. For the metalated samples, the assigned peaks were further cross-checked against the nested IMS-MS datasets for the protonated samples to help eliminate false positives. The validity of the peak assignments for expected metalated products was additionally supported with corresponding increases in population intensity, *m/z*, or drift time shifts, as well as the expected isotopic distribution.

Determination of Experimental Collision Cross Sections

Drift times (t_D) can be converted into collision cross sections using Equation 1 [38],

$$\Omega - \frac{(18\pi)^{1/2}}{16} \frac{ze}{(k_b T)^{1/2}} \left[\frac{1}{m_I} + \frac{1}{m_B}\right]^{1/2} \frac{t_d E}{L} \frac{760}{P} \frac{T}{273.2} \frac{1}{N} \quad (1)$$

where ze is the charge of the ion, k_b is Boltzmann's constant, m_I is the ion mass, m_B is the mass of the buffer gas (He), E is the electric field, L is the drift tube length, P is the pressure, T is the temperature, and N is the neutral number density of the buffer gas at STP. Because the drift tube contains two ion funnels with nonlinear field regions, calculated cross sections are calibrated to well-known systems (e.g., bradykinin and polyalanine). Cross sections can also be determined using the selection gate in the middle funnel region of the instrument, as previously described [52]. Both methods have provided high accuracy in the measurement of cross sections, with values typically determined within ~1 % of

previously reported values for ions believed to be of the same structure [34].

Results and Discussion

Nested IMS-MS Measurements and Observation of Charge-State Families

An example of a nested IMS-MS dataset is displayed in Figure 1 for the protonated and calcium-containing tryptic digestion of equine cytochrome *c*. Distributions of ions generally fall into families within the nested measurements on the basis of the ion charge state and size. The data for protonated tryptic digests primarily show peaks corresponding to doubly-charged peptide ions and, to a lesser extent, singly- and triply-charged ions. The observation of doubly-charged ions is consistent with likely protonation sites at the C-terminal basic residue (lysine or arginine) and the N-terminal amino group. A third proton could be incorporated along the peptide backbone, and is expected for peptides containing missed cleavages (or histidine), which provides a third highly-basic protonation site.

Upon addition of alkaline-earth cations, doubly-charged and triply-charged ions are observed. Unlike protonated systems, triply-charged species are often observed to be the most abundant charge state in the metal-containing systems. This shift in charge distribution might be expected based on the consideration that we have substituted the doubly-charged M^{2+} species for the singly-charged H^+. Where the metal cation resides is much less clear in these systems. Crystallographic studies of metal-containing proteins indicate that metal cations are often coordinated by oxygen-rich functional groups, including backbone carbonyls and residue side chains containing a hydroxyl or carboxylic acid [53]. Additionally, an increasing coordination number is typically observed for cations of increasing size with coordination numbers of 6, 7, and 8 often observed for Mg^{2+}, Ca^{2+}, and Ba^{2+}, respectively [3, 54]. Below, we show that the derived ISPs provide some insight into preferable interactions that occur for metal-containing peptides in the absence of solvent.

Changes in Drift Time upon Substitution of Ca^{2+} for H^+ in Peptide Sequences

It is useful to think of the doubly- and triply-charged metal-containing ions in terms of substituting one H^+ with one M^{2+} ion, yielding $[Pep + M]^{2+}$ and $[Pep + M + H]^{3+}$ species.

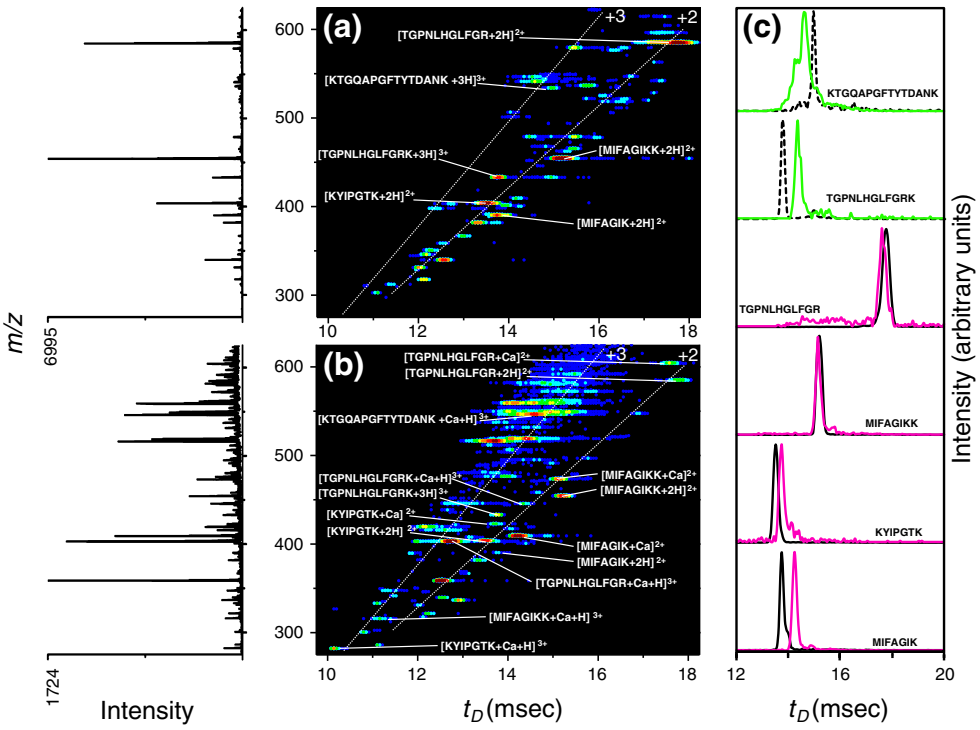

Figure 1. Nested IMS-MS dot plots of the electrosprayed mixture of peptides for the tryptic digestion of equine cytochrome *c*. The sample concentration was ~0.1 mg • mL^{-1} in 50:50 water: acetonitrile solution. Panel (**a**) displays the protonated spectrum and panel (**b**) displays the spectral change upon addition of calcium acetate. Doubly- and triply-charged mobility families are overlayed with white dotted lines. Specific peptides are labeled to display drift and mass shifts upon interaction with Ca^{2+}. Panel (**c**) shows the drift profiles for these specific peptide ions as $[Pep + 2H]^{2+}$ (solid black), $[Pep + Ca]^{2+}$ (solid pink), $[Pep + 3H]^{3+}$ (dashed black), and $[Pep + Ca + H]^{3+}$ (solid green) species. These drift distributions are obtained by integration of all bins at each drift time over a narrow *m/z* range encompassing the monoisotopic mass. Mass spectra are displayed on the left, obtained by integration of all bins at each *m/z* across the entire drift time range

Additionally, to a lesser extent, we observe some $[Pep + 2\,M - H]^{3+}$ species. Here, we focus on the $[Pep + M]^{2+}$ and $[Pep + M + H]^{3+}$ peptide species for elucidation of structural effects upon substitution of M^{2+} for H^+. Each of the tryptic digestions displayed significant differences in the drift time distribution upon addition of metal acetate. From Figure 1 we observe these general differences with drift time distributions for specific calcium-coordinated peptides from the cytochrome *c* digest. In these datasets, the peptide sequences of MIFAGIK, KYIPGTK, MIFAGIKK, and TGPNLHGLFGR are observed as $[Pep + 2H]^{2+}$ and $[Pep + Ca]^{2+}$ species. Variations in the drift distribution are apparent, with the calcium-coordinated MIFAGIK, KYIPGTK, MIFAGIKK, and TGPNLHGLFGR peptides displaying changes of 3.6 %, 1.8 %, –0.4 %, and −1.0 % compared with the respective doubly-protonated species. Metalation also appears to be important in some triply-charged species but not others. As examples, see the drift time distributions for the peptide sequences TGPNLHGLFGRK and KTGQAPGFTYTDANK, observed as the $[Pep + 3H]^{3+}$ and $[Pep + Ca + H]^{3+}$ species. Here, the most intense peaks observed for the $[Pep + Ca + H]^{3+}$ species of TGPNLHGLFGRK and KTGQAPGFTYTDANK change by 4.4 % and −2.4 % compared with the respective triply-protonated species.

It is also common to observe multiple conformer populations for metalated peptide species (where features of lower relative abundance are hereby referred to as minor features). Typically, $[Pep + M]^{2+}$ species favor a single conformer population with minor features generally observed at longer drift times of significantly lower intensity (generally <5 % relative abundance). Broader drift time distributions are often observed for $[Pep + M + H]^{3+}$ species, generally with several peaks of intermediate intensity. The larger number of peaks presumably arises because there are many possible charge site configurations.

Summary of the Alkaline-Earth Cationized Peptide Database

A summary of the derived cross sections for observed conformers of doubly- and triply-charged peptide species observed within the tryptic digest of cytochrome *c* are presented in Table 1. Complete lists of the derived cross sections for all observed doubly- and triply-charged peptide ions can be found in Supplemental Tables 1 and 2, respectively. These tables also provide information regarding peptide sequence, residue length, protein origin, molecular mass, and cross sections for all observed conformers. All cross sections reported here were obtained from data collected concurrently with a previously reported database of alkali metal-containing peptide cross sections, where the accuracy of the reported measurements was assessed [32]. Here, cross sections for 222 doubly- (containing 2 to 14 residues) and 202 triply-charged (containing 4 to 23 residues) peptide ions coordinated with a doubly-charged alkaline-earth cation are reported. A total of 1470 cross section entries (666 doubly- and 804 triply-charged) is provided, of which 1360 cross section entries (581 doubly- and 779 triply-charged) contain a C-terminal lysine or arginine. Of these 1470 cross sections, 455 are charged with a Mg^{2+} (190 $[Pep + Mg]^{2+}$ and 265 $[Pep + Mg + H]^{3+}$), 611 are charged with a Ca^{2+} (291 $[Pep + Ca]^{2+}$ and 320 $[Pep + Ca + H]^{3+}$), and 404 are charged with a Ba^{2+} (185 $[Pep + Ba]^{2+}$ and 219 $[Pep + Ba + H]^{3+}$).

As mentioned above, those metalated peptides that contain an additional proton (i.e., the $[Pep + M + H]^{3+}$ species) often exhibit multiple resolvable mobility peaks. On average, protonated $[Pep + 2H]^{2+}$ ions show ~1.5 peaks for each peptide. Whereas most peptides have two resolvable features, these distributions are still dominated by one large feature. The triply-protonated $[Pep + 3H]^{3+}$ ions display ~1.9 peaks per distribution. One reason for the increase in the number of peaks is that the more highly charged ions are also larger (length and mass) and, thus, can adopt conformations that have substantially different structures that allow them to be resolved. Localization of the H^+ at the various basic sites offered by these tryptic peptide ions also could contribute to the increase in the number of peaks.

The distributions for metal-containing peptides are often more complicated than their protonated counterparts. Often, several peaks with similar intensities are observed. On average, $[Pep + Mg]^{2+}$ species show ~1.6 peaks, and this increases to ~2.4 for $[Pep + Mg + H]^{3+}$). The $[Pep + Ca]^{2+}$ species average ~1.7 peaks per mobility distribution, and this increases to ~2.2 for the triply-charged $[Pep + Ca + H]^{3+}$ forms. Similarly, distributions for the barium-coordinated $[Pep + Ba]^{2+}$ species contain ~1.6 peaks per spectrum, and this value increases to ~2.1 for $[Pep + Ba + H]^{3+}$ ions.

Range of Cross Sections for Species with Similar Masses

At a given mass, triply-charged species exhibit a larger range of cross sections than their doubly-charged counterparts. Figure 2 shows a comparison of cross sections to molecular weight for $[Pep + Ba]^{2+}$ or $[Pep + Ba + H]^{3+}$ species with doubly- or triply-protonated species, respectively. Cross sections increase with molecular mass for both the doubly- and triply-charged species. However, the range of values at a given mass is significantly different for the doubly- and triply-charged populations. For the $[Pep + M]^{2+}$ species, the range of cross sections is relatively constant, with a standard deviation of ±3.6 % over the entire dataset. Such a narrow range may suggest that structures are relatively similar for these doubly-charged metal-containing species.

A much larger range is observed for the intense features of $[Pep + M + H]^{3+}$ species. At m ~1000, cross sections vary by±10 % as Coulombic repulsion between the two cations may result in more extended conformations. As m increases (and thus the number of amino acid residues), additional functional groups become available for interaction

Table 1. Cross Sections for Doubly- and Triply Charged Peptides from Tryptic Digest of Equine Cytochrome *c*[a]

Residue Length	Assigned sequence[b]	Molecular Mass[c]	Cross section (Å2)[d]							
			$[M + 2H]^{2+}$	$[M + Mg]^{2+}$	$[M + Ca]^{2+}$	$[M + Ba]^{2+}$	$[M + 3H]^{3+}$	$[M + Mg + H]^{3+}$	$[M + Ca + H]^{3+}$	$[M + Ba + H]^{3+}$
5	GGKHK	525.30	**163.2**							
5	GITWK	603.34	**167.8**	**182.2**	**185.9**	**188.4**				
						201.5				
5	IFVQK	633.39	**183.5**	**181.3**	**196.1**	**201.5**				
						211.8				
5	KATNE	561.28		**161.0**	**163.7**	**166.0**				
5	KKTER	660.39	**181.7**	**179.5**	**182.2**					**219.7**
6	KIFVQK	761.48	**201.9**	**209.1**		**216.4**			**230.3**	**240.7**
			207.5							
6	YIPGTK	677.37	**190.0**	**185.9**	**190.6**	**193.1**				
			183.5			*214.6*				
7	GDVEKGK	731.38	**196.4**		**207.2**					
7	KYIPGTK	805.47	**204.7**	**209.1**	**209.1**	**209.0**		**235.9**	**230.3**	**235.1**
7	MIFAGIK	778.44	**208.4**	**211.8**	**216.5**	218.3				
				218.3	*226.6*					
8	MIFAGIKK	906.54	**230.5**		**230.3**	**235.1**		**245.6**	**253.9**	**274.2**
					239.6			*263.6*	*259.5*	*253.3*
9	EDLIAYLKK	1091.62	**253.6**							
9	MIFAGIKKK	1034.63	**249.0**				**276.6**			
11	TGPNLHGLFGR	1167.61	**270.2**	**275.7**	**268.3**	**270.5**		**283.1**	**290.0**	**295.2**
								310.8	*273.4*	
									281.7	
12	TGPNLHGLFGRK	1295.71	**282.2**				**312.6**	**299.7**	**327.5**	**293.8**
			277.6				*340.3*	*306.7*		*303.6*
								312.2		
13	HKTGPNLHGLFGR	1432.77	**307.1**				**351.3**	**326.1**	**341.4**	
							329.2			
14	HKTGPNLHGLFGRK	1560.86					**376.2**			
14	TGQAPGFTYTDANK	1469.68	**298.8**		**301.6**	**298.5**		**328.9**		**313.4**
								312.2		
15	KTGQAPGFTYTDANK	1597.77	**315.4**				**340.3**	**334.4**	**333.0**	**337.2**
			317.2					*328.9*	*316.4*	
									327.5	
									344.1	
16	GGKHKTGPNLHGLFGR	1674.91							**348.3**	
16	TGQAPGFTYTDANKNK	1711.82						**341.4**	**342.7**	
								355.2		
17	KTGQAPGFTYTDANKNK	1839.91					**398.3**	**364.9**	**363.6**	
18	GITWKEETLMEYLENPKK	2208.11					**450.9**			

[a]All values were measured using a coupled ion-mobility time-of-flight home-built instrument for analysis of complex peptide mixtures from a tryptic digestion. See text and references for full descriptions of the instrument and digestion protocol. For simplicity of comparison, peptides listed here are of amino acid residue length 5 and above. Peptides of residue length less than 5 were observed as doubly-charged species and are included within the supplemental tables supplemental tables.

[b]Peptide sequences were expected from tryptic digests and generated using the Peptide Mass tool at http://expasy.org/tools/peptide-mass.html

[c]The molecular mass is reported as the monoisotopic mass of the peptide without any ionizing species.

[d]Cross sections are reported for measurements specific to the peptide ion species. The most intensely observed conformer is listed first and bolded. Additional observed minor features are listed beneath and italicized.

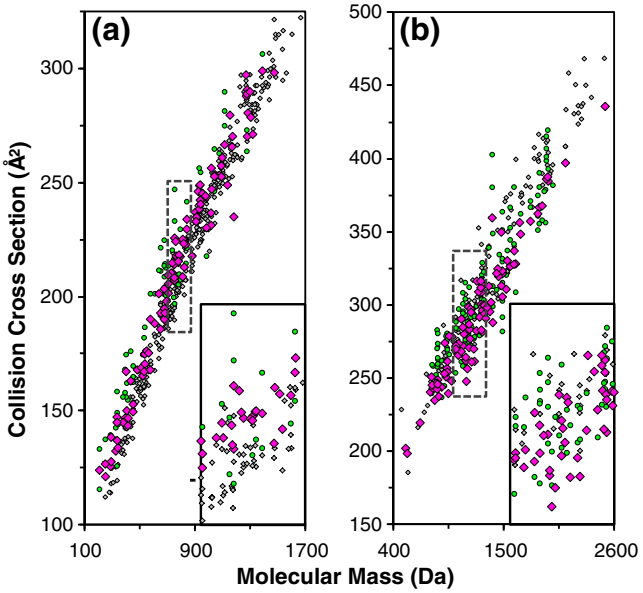

Figure 2. Cross sections as a function of molecular mass for all tryptic peptide ions that are protonated or charged by Ba^{2+}. Doubly-charged peptide ions ($[Pep + 2H]^{2+}$ as compared with $[Pep + Ba]^{2+}$) and triply-charged peptide ions ($[Pep + 3H]^{3+}$ compared with $[Pep + Ba + H]^{3+}$) are shown in panels (**a**) and (**b**), respectively. Protonated ions (gray diamonds) and barium-coordinated ions (pink diamonds) are displayed with minor features for the barium-coordinated species (green circles). Insets are provided (defined by the overlayed gray dashed box) to display an expanded view of the range of cross sections observed for a given molecular mass

with the metal cation. The range of values associated with major features decreases with increasing m, resulting in a range of ±7 % at m ~1500 and ±5 % at m ~2000. This may result from a more globular peptide structure at larger masses with a smaller effect from charge solvation. Figure 2 shows that minor features also exist over a wide distribution of cross sections (for a given value of m). Similar comparative plots for the doubly- and triply-charged peptide ions containing Mg^{2+} or Ca^{2+} are provided in Supplemental Figures 1 and 2, respectively. Overall, the trends in these metal systems are similar to those described here for Ba^{2+}.

Variations in Cross Section with Cation Size

Figure 2 also provides some insight about general trends regarding the relationship of overall cross section with differences in the cation sizes. The ionic radii for alkaline-earth cations are $r(Mg^{2+})=0.72$ Å, $r(Ca^{2+})=1.00$ Å, and $r(Ba^{2+})=1.35$ Å (coordination number of 6) [55]. The ionic radii for these cations increase if larger coordination numbers are considered. For the intense features of $[Pep + M]^{2+}$ peptide ions, the average cross sections increase with increasing cation size. Compared with $[Pep + 2H]^{2+}$ species, these $[Pep + M]^{2+}$ ions are slightly larger in size [i.e., average increases of 1.4±7.9 Å^2 (Mg^{2+}), 4.0±7.6 Å^2 (Ca^{2+}), and 6.5±9.2 Å^2 (Ba^{2+}), corresponding to a percentage change of 0.9 %±4.2 %, 2.4 %±4.0 %, and 3.8 %±5.0 %, respectively, for the data in Figure 2]. Compared with observed $[Pep + 2H]^{2+}$ species, larger $[Pep + M]^{2+}$ cross sections are observed for larger fractions of the metal containing species according to increased ionic radii [i.e., the percentage of metal containing ions having a larger cross section is as follows: 60.6 % (Mg^{2+}), 73.9 % (Ca^{2+}), and 79.6 % (Ba^{2+}) of the metal-containing species]. Presumably, the doubly-charged metalated peptides are relatively compact because the tight interactions of M^{2+} with peptide functional groups [12]. The large deviations noted for these changes in cross section upon metalation indicate that the metals have a significant influence on the overall peptide structure for many of these peptides.

Finally, we note that cross sections decrease with increasing ionic size for the intense features of $[Pep + M + H]^{3+}$ peptide ions. Compared with $[Pep+3H]^{3+}$ species, the $[Pep + M + H]^{3+}$ cross sections are significantly smaller by an average of 14.8±13.7 Å^2 (Mg^{2+}), 16.5±15.8 Å^2 (Ca^{2+}), and 18.5±17.7 Å^2 (Ba^{2+}), corresponding to a respective percentage decreases of 4.4 %±4.8 %, 4.9 %±4.4 %, and 5.5 %±5.0 %. Smaller cross sections for the intense features of $[Pep + M + H]^{3+}$ peptide ions are observed for 87.0 % (Mg^{2+}), 83.9 % (Ca^{2+}), and 88.1 % (Ba^{2+}) compared with the respective $[Pep + 3H]^{3+}$ species. These decreases are primarily clustered at masses between 800 and 1600 (generally corresponding to an amino acid residue length of 7 to 15). We speculate that the broader distributions of structures are related to the ability of larger alkaline-earth cations to accommodate larger coordination numbers. An increased coordination number may lead to a larger portion of the peptide solvating the metal cation, resulting in a more compact conformation.

Derivation of Intrinsic Size Parameters for Individual Amino Acids

The assembly of such large datasets of peptide ion species makes it possible to evaluate the role of the metal cation in establishing the structure for a gas-phase peptide ion. As such, generalizations associated with these metal-mediated structures can be assessed to relate the interaction of the metal cation with specific amino acid residues. These interactions can be elucidated with the use of intrinsic size parameters (ISP), of which derivations are made by relating the occurrence frequency of individual amino acid residues with the cross section deviation from the population mean. The utility of such an analysis has been demonstrated with a previously reported database of alkali-containing peptide ions [32] with these ISPs displaying a preference for the metal to interact with polar aliphatic amino acid residues and methionine.

To begin, differences in cross section originating from mass are removed with a normalization by a second-order polynomial fit relating the cross section to the molecular mass for each $[Pep + M]^{2+}$ population. The normalized

value is obtained as a ratio of the experimental cross section to the polynomial fit cross section and is termed the reduced cross section. As noted previously, the reduced cross section can be used to decipher differences in cross section associated with amino acid composition [32, 34, 36]. Original reduced cross section calculations utilized a polynomial relating cross section to mass for singly-protonated polyalanine peptide ions, allowing comparison to a globular (sphere-like) conformation. However, the relationship between molecular mass and collision cross section is unique for each peptide ion species, primarily characterized by ionic size, ionic charge, coordination number and geometry, and the number of charge carriers. As such, it is more instructive to utilize a molecular weight fit for the calculation of reduced cross sections [32, 33]. Reduced cross sections calculated for the $[Pep + M]^{2+}$ datasets range from 0.93 to 1.12 for Mg^{2+}, 0.91 to 1.09 for Ca^{2+}, and 0.87 to 1.11 for Ba^{2+}.

ISP values are calculated by relating the reduced cross sections with a matrix of the product of size parameters and the occurrence frequency for each amino acid residue intrinsic to each peptide sequence, as defined by Equation 2 [34, 36]:

$$\Sigma_{j=1}^{n} X_{ij} p_j = y_i \quad (2)$$

Here, i corresponds to each unique peptide sequence comprising the dataset and j corresponds to each amino acid present within the population set [20 in these data, with Cys modified during the digestion protocol by a carboxyamidomethyl protecting group (hereafter denoted as Cys* or C*)]. The variable X_{ij} refers to the frequency of occurrence of each residue j in each sequence i. The variable p_j refers to the unknown parameters for each residue j and is the variable determined from these datasets. The sum of the products of the occurrence frequency of each residue and the unknown residue parameters are equated to the variable y_i, which corresponds to the reduced cross section for each sequence i. Each equation provides a relationship between the product of residue frequencies and the unknown size parameters with each measured reduced cross section. This system of equations is solved for the best fit ISP values (p_j) using a linear least-squares regression analysis [56]. Uncertainties for each derived parameter are calculated as the square root of the variance and are representative of one standard deviation.

Comparisons of ISP Values from Peptides Containing Different Metals

The derived ISPs for protonated and metalated species are listed in Table 2. Only the observed major features were utilized in these derivations. In general, ISPs derived for these different systems are similar. Values for nonpolar aliphatic residues are relatively large (from 0.95 to 1.22), whereas values for polar aliphatic residues are small (0.77 to 1.02). Intermediate ISP values are observed for aromatic residues (0.88 to 1.12). The errors reported for the $[Pep + Ba]^{2+}$ species are larger than the $[Pep + Mg]^{2+}$ or $[Pep + Ca]^{2+}$ species. This is interesting, considering the similar number of measurements included within the datasets. We interpret this as evidence of increased structural diversity within the $[Pep + Ba]^{2+}$ species, possibly because of a variance in coordination number to accommodate the larger cation size.

At first glance, it appears that the alkaline-earth cations influence the specific amino acid residues similarly to alkali cations. That is, trends in ISP values for nonpolar aliphatic, aromatic, and polar aliphatic residues are similar for both types of ions. However, upon closer inspection, we do observe differences. For example, the ISPs for the nonpolar aliphatic residues (Ala, Val, Ile, Leu, and Met), aromatic residues (Phe, Tyr, and Trp) as well as Asp are generally smaller for the $[Pep + M]^{2+}$ species than those observed for the alkali $[Pep + M + H]^{+}$ species. ISPs for most polar aliphatic residues (Glu, Asn, Gln, Ser, Thr) as well as Pro, however, are larger for these alkaline-earth-coordinated species compared with the alkali species.

Insight into the Interactions of Alkaline-Earth Cations with Specific Amino Acids

Figure 3 shows a relative difference plot of ISPs upon substitution of M^{2+} for H^{+} (i.e., $\frac{ISP_{[Pep+M]^{2+}} - ISP_{[Pep+H]^{+}}}{ISP_{[Pep+H]^{+}}}$). The $[Pep + H]^{+}$ ISPs used in this analysis were derived using the singly-protonated cross section database (absent Cys-containing peptide ions) provided by Valentine et al. [34] Compared with alkali-containing tryptic peptide ions, the alkaline-earth ISP values suggest that these specific amino acid residue interactions are less pronounced [32]. This can be observed by comparing the panels in Figure 3 for the alkaline-earth- and alkali-containing ISPs. Based on the alkali series, we anticipated increased contributions to cross sections for the nonpolar aliphatic and aromatic residues [36]. Overall, this is the case. However, a residue size dependence is observed for the nonpolar aliphatic residues. For example, the ISP for Ala is relatively small. As the length of the side chain increases, the contribution to cross section also increases. These results suggest that the alkaline-earth metal cations interact less specially with specific side chains than the alkali metal ions. Presumably the M^{2+} species interacts with oxygen or (to a lesser degree) with nitrogen atoms on the peptide backbone [57].

The polar aliphatic residues of Asp, Ser, and Thr, all show relatively small ISP values. These values are ~13 %, ~7 %, and ~4 % smaller than values observed in the protonated system, respectively. Pro and Gly also show smaller ISP values, presumably by distortion of the peptide backbone to enable interaction of the M^{2+} with other peptide functional groups. The aromatic residues generally show larger ISP values (by values up to ~7 %). Similarly, His shows a larger ISP (by values up to ~5 %). Of the aromatic residues, smaller ISP

Table 2. Intrinsic Size Parameters of Individual Amino Acid Residues for Peptide Ion Species[a]

Residue		Parameterization set								
		Protonated		Alkali-coordinated				Alkaline-Earth-coordinated		
		$[Pep+H]^{+}$[b]	$[Pep+2H]^{2+}$[c]	$[Pep+Li+H]^{2+}$[d]	$[Pep+Na+H]^{2+}$[e]	$[Pep+K+H]^{2+}$[f]	$[Pep+Cs+H]^{2+}$[g]	$[Pep+Mg]^{2+}$[h]	$[Pep+Ca]^{2+}$[i]	$[Pep+Ba]^{2+}$[j]
Nonpolar aliphatic	Ala	1.02 (0.01)	0.98 (0.01)	1.00 (0.03)	1.03 (0.03)	1.00 (0.03)	1.07 (0.04)	0.96 (0.02)	0.98 (0.01)	0.97 (0.02)
	Val	1.05 (0.01)	1.05 (0.02)	1.07 (0.03)	1.10 (0.04)	1.18 (0.03)	1.08 (0.04)	1.03 (0.02)	1.06 (0.02)	1.04 (0.03)
	Ile	1.08 (0.01)	1.08 (0.02)	1.11 (0.05)	1.10 (0.05)	1.22 (0.04)	1.11 (0.06)	1.06 (0.03)	1.08 (0.02)	1.07 (0.03)
	Leu	1.14 (0.01)	1.13 (0.02)	1.17 (0.03)	1.20 (0.03)	1.18 (0.03)	1.14 (0.03)	1.16 (0.02)	1.16 (0.01)	1.17 (0.02)
	Met	1.02 (0.03)	1.17 (0.04)	0.95 (0.09)	0.96 (0.08)	1.12 (0.08)	1.02 (0.10)	1.03 (0.05)	1.07 (0.04)	0.97 (0.07)
Aromatic	Phe	1.04 (0.01)	1.01 (0.02)	1.09 (0.05)	1.11 (0.04)	1.07 (0.04)	1.09 (0.05)	1.07 (0.03)	1.04 (0.02)	1.01 (0.03)
	Tyr	0.98 (0.02)	0.98 (0.03)	0.94 (0.05)	1.10 (0.07)	1.12 (0.07)	0.99 (0.07)	1.02 (0.04)	1.02 (0.03)	0.88 (0.03)
	Trp	1.00 (0.03)	0.95 (0.04)	1.08 (0.09)	1.00 (0.07)	1.03 (0.07)	0.93 (0.09)	0.97 (0.04)	0.99 (0.04)	0.97 (0.08)
Polar aliphatic	Asp	0.89 (0.01)	0.91 (0.03)	1.02 (0.06)	0.91 (0.06)	1.01 (0.06)	0.87 (0.08)	0.84 (0.04)	0.85 (0.03)	0.77 (0.05)
	Glu	0.94 (0.01)	0.94 (0.02)	0.93 (0.04)	0.88 (0.04)	0.93 (0.03)	0.91 (0.05)	0.92 (0.03)	0.94 (0.02)	0.90 (0.04)
	Asn	0.93 (0.02)	0.92 (0.03)	0.91 (0.06)	0.90 (0.05)	0.87 (0.05)	0.91 (0.07)	0.92 (0.03)	0.92 (0.02)	0.92 (0.05)
	Gln	0.95 (0.02)	0.96 (0.03)	0.90 (0.06)	0.91 (0.05)	0.88 (0.05)	0.89 (0.06)	0.94 (0.05)	0.96 (0.03)	0.95 (0.05)
	Ser	0.99 (0.02)	0.96 (0.02)	0.91 (0.05)	0.90 (0.05)	0.98 (0.04)	0.99 (0.06)	0.97 (0.03)	0.92 (0.02)	0.92 (0.05)
	Thr	0.99 (0.01)	0.93 (0.02)	1.02 (0.04)	0.93 (0.04)	0.94 (0.04)	1.02 (0.05)	0.96 (0.03)	0.95 (0.02)	0.99 (0.03)
	Pro	0.97 (0.02)	0.99 (0.02)	0.91 (0.05)	0.87 (0.05)	0.92 (0.05)	0.85 (0.06)	0.95 (0.03)	0.94 (0.03)	0.93 (0.04)
	Gly	0.97 (0.01)	0.93 (0.02)	0.91 (0.03)	0.97 (0.03)	0.93 (0.03)	0.99 (0.04)	0.91 (0.03)	0.96 (0.02)	0.99 (0.03)
	His	0.94 (0.02)	1.07 (0.03)	0.99 (0.06)	1.03 (0.06)	0.96 (0.05)	0.79 (0.07)	0.97 (0.03)	0.99 (0.03)	0.98 (0.04)
	Cys*		0.95 (0.03)	0.73 (0.07)	0.94 (0.08)	0.87 (0.07)	0.85 (0.08)	0.95 (0.05)	0.87 (0.04)	0.99 (0.11)
	Lys	0.98 (0.01)	0.98 (0.02)	0.95 (0.04)	0.97 (0.05)	0.84 (0.05)	0.97 (0.06)	0.98 (0.02)	0.98 (0.02)	1.01 (0.02)
	Arg	0.97 (0.01)	1.06 (0.03)	0.99 (0.06)	0.82 (0.08)	0.81 (0.07)	0.96 (0.09)	1.09 (0.04)	1.03 (0.02)	1.00 (0.03)

[a]The amino acid size parameters were derived by solving a system of equations that relate the occurrence frequency of each amino acid and the unknown size parameters to a reduced cross section of each peptide (see text). Uncertainties, given in parenthesis, correspond to one standard deviation about the mean. Elevated errors are generally observed for residues of decreased frequency (such as Met, Trp, His, or Cys*) but are also attributed to structural variation in the datasets resulting from differences in charge site or cation coordination number. Cys* (or C*) refers to the carboxyamidomethylation modification of the Cys thiol group during the trypsin digestion protocol.

[b]Amino acid size parameters derived from 408 peptides having the form $[Xxx_nLys/Arg + H]^+$, as provided by a database from Valentine, *et al*., 1999 [34]. Here, Xxx is any naturally occuring amino acid (all naturally occuring amino acids, absent Cys) and n=1 to 14. The second-order polynomial of Ω=4.092E-5x^2+0.2396x + 39.6675, where x is the molecular mass, was used to generate reduced cross sections. The ISP for Cys* is not presented due to a lack of this modified residue within the [Pep + H] + peptide ion cross sections (9 peptides containing unmodified Cys were discarded in this derivation).

[c]Amino acid size parameters derived from major features of 284 peptides having the form $[Xxx_nLys/Arg + 2H]^{2+}$, as provided by a database from Dilger, *et al.*, 2012 [32]. Here, Xxx is any naturally occuring amino acid and n=4 to 16 (except for Cys, which is carboxyamidomethylated). The second-order polynomial of Ω=-1.334E-5x^2+0.1798x+74.2775, where x is the molecular mass, was used to generate reduced cross sections.

[d]Amino acid size parameters derived from major features of 95 peptide ions having the form $[Xxx_nLys/Arg + Li + H]^{2+}$, as provided by a database from Dilger, *et al.*, 2012 [32]. Here, Xxx is any naturally occuring amino acid (except for Cys, which is carboxyamidomethylated) and n=4 to 14. Reduced cross sections were generated by division of the observed cross section with the second-order polynomial of Ω= −1.440E-5x^2+0.1736x+81.9521, where x is the molecular mass.

[e]Amino acid size parameters derived from major features of 105 peptide ions having the form $[Xxx_nLys/Arg + Na + H]^{2+}$, as provided by a database from Dilger, *et al.*, 2012 [32]. Here, Xxx is any naturally occuring amino acid (except for Cys, which is carboxyamidomethylated) and n=4 to 15. Reduced cross sections were generated by division of the observed cross section with the second-order polynomial of Ω=-2.387E-5x^2+0.2039x+63.5933, where x is the molecular mass.

[f]Amino acid size parameters derived from major features of 92 peptide ions having the form $[Xxx_nLys/Arg + K + H]^{2+}$, as provided by a database from Dilger, *et al.*, 2012 [32]. Here, Xxx is any naturally occuring amino acid (except for Cys, which is carboxyamidomethylated) and n=4 to 15. Reduced cross sections were generated by division of the observed cross section with the second-order polynomial of Ω=-2.560E-5x^2+ 0.2042x+68.3009, where x is the molecular mass.

[g]Amino acid size parameters derived from major features of 70 peptide ions having the form $[Xxx_nLys/Arg + Cs + H]^{2+}$, as provided by a database from Dilger, *et al.*, 2012 [32]. Here, Xxx is any naturally occuring amino acid (except for Cys, which is carboxyamidomethylated) and n=4 to 15. Reduced cross sections were generated by division of the observed cross section with the second-order polynomial of Ω=-1.810E-5x^2+0.1836x+83.6551, where x is the molecular mass.

[h]Amino acid size parameters derived from major features of 113 peptide ions having the form $[Xxx_nLys/Arg + Mg]^{2+}$. Here, Xxx is any naturally occuring amino acid (except for Cys, which is carboxyamidomethylated) and n=1 to 13. Reduced cross sections were generated by division of the observed cross section wi th the second-order polynomial of Ω=-1.573E-5x^2+0.1820x+75.5546, where x is the molecular mass.

[i]Amino acid size parameters derived from major features of 160 peptide ions having the form $[Xxx_nLys/Arg + Ca]^{2+}$. Here, Xxx is any naturally occuring amino acid (except for Cys, which is carboxyamidomethylated) and n=1 to 13. Reduced cross sections were generated by division of the observed cross section with the second-order polynomial of Ω=-2.948E-5x^2+0.2012x+72.2022, where x is the molecular mass.

[j]Amino acid size parameters derived from major features of 110 peptide ions having the form $[Xxx_nLys/Arg + Ba]^{2+}$. Here, Xxx is any naturally occuring amino acid (except for Cys, which is carboxyamidomethylated) and n=1 to 13. Reduced cross sections were generated by division of the observed cross section with the second-order polynomial of Ω=-4.258E-5x^2+0.2184x+71.0911, where x is the molecular mass.

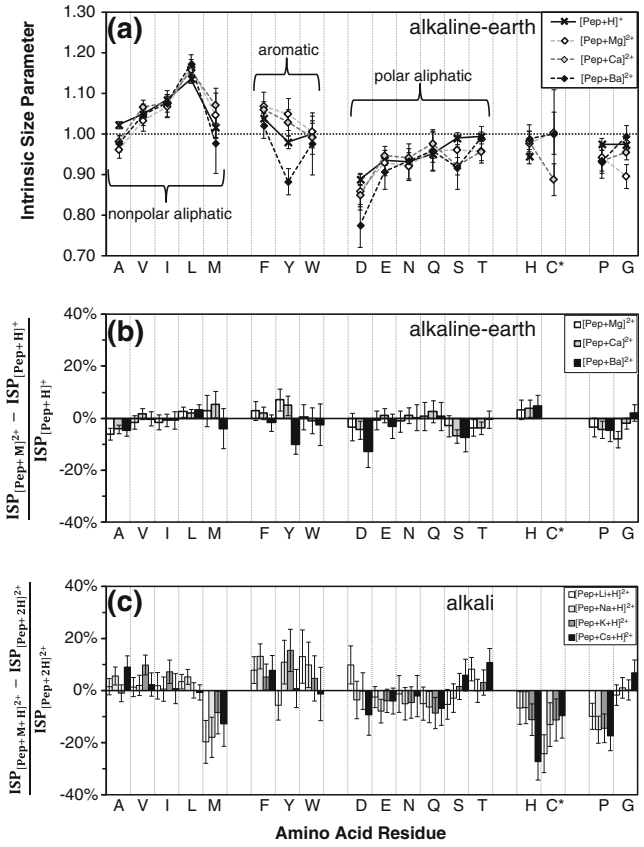

Figure 3. Relative difference plots of the ISP values for specific amino acid residues for the $[Pep + M]^{2+}$ species as compared to $[Pep + H]^{+}$ species. Panel (**a**) displays the plot of the ISP values for $[Pep + H]^{+}$ and $[Pep + M]^{2+}$ species used in the relative difference calculations. White, gray, and black diamonds (with dashed lines) correspond to M^{2+}=Mg^{2+}, Ca^{2+}, and Ba^{2+}, respectively. Black crosses (with solid lines) correspond to the ISP values for $[Pep + 2H]^{2+}$ species. Error bars represent one standard deviation about the mean. Panel (**b**) shows the relative difference in alkaline-earth ISPs with white, gray, and black bars corresponding to M^{2+}=Mg^{2+}, Ca^{2+}, and Ba^{2+}, respectively. Comparisons of Cys* are not presented due to a lack of this modified residue within the $[Pep + H]^{+}$ peptide ion cross sections provided by Valentine et al. [34]. Panel (**c**) shows the relative difference in alkali ISPs with white, medium gray, dark gray, and black bars corresponding to M^{+}=Li^{+}, Na^{+}, K^{+}, and Cs^{+}, respectively [32]. Uncertainties are displayed as vertical error bars and are calculated as the square root of the product sum of the squared errors and their partial derivatives. The ISPs presented here are derived by maintaining Lys and Arg ISP values equivalent to those derived from the respective protonated parameterization sets

values are displayed only by coordination with Ba^{2+} (particularly with Tyr by ~10 %). It is possible that the larger size of Ba^{2+} enables a more effective interaction with the hydroxyl group of Tyr. It is noted, however, that pi-solvation effects specifically by Ba^{2+} with Phe are reported [23]. The plot of the individual ISPs used in the alkaline-earth structural analysis accentuates the subtle differences noted between the metalated and protonated systems.

Comparison of Metalated ISPs with Metal-Binding Sites in Known Protein Systems

Data mining of detailed crystal structures of metalloproteins indicates the binding preferences of biologically relevant metals (Na^{+}, K^{+}, Mg^{2+}, and Ca^{2+}) with specific amino acid residues [53]. Our interpretations of the large ISP values for aromatic and nonpolar aliphatic residues agree that the frequency of metal-residue interactions is limited for these residues. A difference is observed for alkali cations and the sulfurous moiety of Met (as well as Cys). These residues appear to interact strongly with the metals in the gas phase, but not in the crystallography data. Our interpretation of metalated ISPs also agrees with interactions of alkali metals with all polar aliphatic residues as well as alkaline-earth metals with the polar residues of Asp, Glu, and Asn (as well as Ser and Thr, specifically with magnesium) from the crystallography data. In addition to the specificity of these metal-residue interactions, it is interesting that relative binding preferences for specific residues are similar in both the ISP analysis and the crystallography data. A difference is noted, however, with the limited frequency of interaction of alkaline-earth metals with the main chain (backbone) functional groups reported in the crystallography data (all normalized frequency values reported for Mg^{2+} and Ca^{2+} with the main chain oxygen or nitrogen are less than 1.5). Our interpretation of the alkaline-earth ISPs suggests an interaction of the metal cation with the backbone functional groups. One final disagreement is noted for the frequency of interaction for magnesium with histidine. Presumably, the differences noted here are attributed to the metal-peptide system providing a relatively limited number of functional groups to solvate the M^{2+}. As such, the metal–residue interactions described here are more generalized compared with the evolutionarily-specialized metalloproteins comprising the crystallography data.

Application of ISP Values for Prediction of Cross Sections

ISP values can be used to estimate cross sections. Typically, MS-MS techniques are used for identification of a peptide sequence, although false identifications often persist [37]. Complementary mobility-derived ISP values offer an independent means of improving the confidence of these peptide ion assignments [33]. Figure 4 shows the ratios of the retrodicted and experimental reduced cross sections for both the ISP fit and the molecular weight fit. Improvements of estimation of cross section are shown for each of the $[Pep + M]^{2+}$ ISPs, with cross sections within ±2 % of experimental values for 66 % of $[Pep + Mg]^{2+}$ peptide ions (75 of 113 cross sections), 70 % of $[Pep + Ca]^{2+}$ peptide ions (112 of 160 cross sections), and 61 % of $[Pep + Ba]^{2+}$ peptide ions

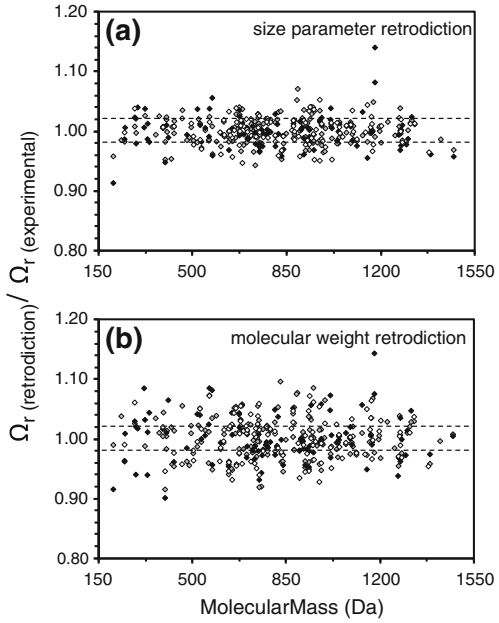

Figure 4. Prediction accuracy scatter plot for 113 $[(Xxx)_nLys/Arg + Mg]^{2+}$ (white diamonds), 160 $[(Xxx)_nLys/Arg + Ca]^{2+}$ (gray diamonds), and 110 $[(Xxx)_nLys/Arg + Ba]^{2+}$ (black diamonds) peptide ions. Here, Xxx is any naturally occurring amino acid (where cysteine is modified with a carboxymethylated protecting group) and n=1 to 13. Retrodictions produced by ISPs are displayed in panel (**a**) with those produced by a second-order polynomial regression relating molecular weight to cross section in panel (**b**). Dotted lines are overlayed on the plots to display where retrodicted values agree within 2 % of experimentally measured results

(67 of 110 cross sections). This is in contrast to the retrodictive ability of the molecular weight fit, as cross sections are within ±2 % of experimental values for 42 % of $[Pep + Mg]^{2+}$ peptide ions (47 of 113 cross sections), 47 % of $[Pep + Ca]^{2+}$ peptide ions (75 of 160 cross sections), and 46 % of $[Pep + Ba]^{2+}$ peptide ions (51 of 110 cross sections). Variances of the retrodictions using ISPs as compared to the molecular weight fit significantly decrease by 58 % [$F(1,109)$= 2.01, P<0.001], 60 % [$F(1,159)$=2.48, P<0.001], and 50 % [$F(1,112)$=2.37, P<0.001] for the respective $[Pep + Mg]^{2+}$, $[Pep + Ca]^{2+}$, and $[Pep + Ba]^{2+}$ species.

Probing of structural elements of $[Pep + M + H]^{3+}$ peptide ions using $[Pep + M]^{2+}$ and $[Pep + 2H]^{2+}$ ISPs

The ISP values are descriptive of the general interactions that govern structure within the metalated and protonated systems as well as the overall sizes of the amino acid residues. As such, it is interesting to consider using these ISPs as a structural probe for the multiple conformers typically observed for $[Pep + M + H]^{3+}$ peptide species. Here we apply the ISPs derived from the $[Pep + M]^{2+}$ and $[Pep + 2H]^{2+}$ species to query the $[Pep + M + H]^{3+}$ conformers. Those conformers predicted with the $[Pep + M]^{2+}$ ISPs are assumed to contain elements of structure that arise by specific metal-residue interactions. Similarly, conformers predicted by the $[Pep + 2H]^{2+}$ ISPs presumably arise from solvation of the protons and the repulsive Coulombic forces exhibited by the dual charge carriers.

Figure 5 shows the experimental reduced cross sections at a given molecular mass for the $[Pep + Ca + H]^{3+}$ species. As discussed previously, the range of reduced cross sections is larger for ions of smaller masses resulting primarily from Coulombic repulsion of the two cations. ISPs derived from the $[Pep + M]^{2+}$ and $[Pep + 2H]^{2+}$ species are used to predict a reduced cross section for each peptide sequence observed within the $[Pep + M + H]^{3+}$ species. This prediction is then compared with the empirical reduced cross section. For the $[Pep + Ca + H]^{3+}$ species, ~66 % have a reduced cross section that is predicted within ±2 % (94 of the 142 peptide sequences). Similar results are predicted for the $[Pep + Mg + H]^{3+}$ and $[Pep + Ba + H]^{3+}$ species [~73 % of magnesium-containing species (80 of 109 peptide sequences) and ~74 % of barium-containing species (76 of 103 peptide sequences)]. Additionally, most of these predicted measurements are major features. For example, 71 of the 94 predicted $[Pep + Ca + H]^{3+}$ conformers are observed as the most abundant feature in the drift distribution.

Those measurements predicted within±2 % by both the $[Pep + M]^{2+}$ and $[Pep+2H]^{2+}$ ISPs are generally clustered around the midline of the distribution (reduced cross section of 1.0). Conformers predicted only by the $[Pep + M]^{2+}$ ISPs are structurally more compact (12 of 17 reduced cross sections predicted below the midline). Conversely, conformers predicted only by the $[Pep + 2H]^{2+}$ ISPs are

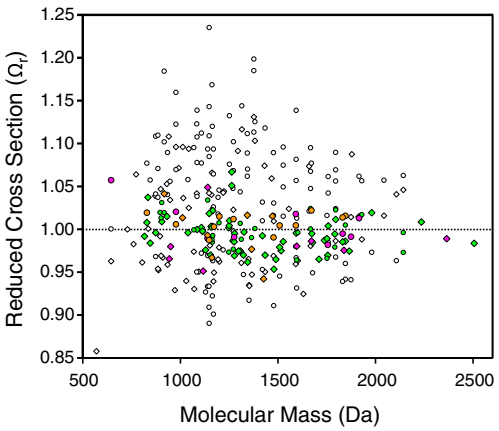

Figure 5. Experimental reduced cross sections for all observed $[Pep + Ca + H]^{3+}$ major features (diamonds) and minor features (circles). Reduced cross sections are predicted within ±2 % by the derived $[Pep + Ca]^{2+}$ ISPs (pink), $[Pep + 2H]^{2+}$ ISPs (orange), or by both ISP parameterization sets (green). Reduced cross sections are calculated by division of each measurement to a second-order polynomial relating cross section and molecular mass for the $[Pep + Ca + H]^{3+}$ major features (Ω=9.78E-6x^2+0.1028x+150.3397, where x is the molecular mass of the ion)

generally more elongated (14 of 20 reduced cross sections clustered above the midline). Similar trends are noted for the magnesium- and barium-containing species.

There also exists a population of conformers that are either more compact or more elongated (largely of minor features) that are not accurately predicted by either set of ISPs. Structures that are more compact could arise from higher coordination numbers of the metal cation. Additional elongated structures are expected as the triply-charged peptide experiences a larger Coulombic repulsion between the M^{2+} and H^{+}. In both cases, the influence of the metal cation on peptide structure is altered through a change in the interactions associated with solvation of both charge carriers.

Summary and Conclusions

This work presents a database containing 1470 cross section entries of peptide ions containing alkaline-earth metals (Mg^{2+}, Ca^{2+}, and Ba^{2+}) in the $[Pep + M]^{2+}$ and $[Pep + M + H]^{3+}$ charge configurations. Cross sections were calculated from IMS-MS measurements of tryptic digestions of 24 proteins. This large number of values allows for generalizations on peptide structure resulting from the coordination of an alkaline-earth cation. Cross sections for $[Pep + M]^{2+}$ peptide ions are larger with increasing cation size. However, $[Pep + M + H]^{3+}$ peptide ions often exhibit multiple resolvable conformers with cross sections of major features that decrease with increasing metal cation size.

Interactions between the metal cation and specific amino acid residues were probed using ISP derivations. The ISPs presented here display general charge solvation effects similar to those previously derived for protonated [32–34, 36] or alkali-coordinated [32] peptide ion species. Specifically, ISP values are generally larger for nonpolar aliphatic residues, intermediate for aromatic residues, and smaller for polar aliphatic residues. Analysis of the relative difference of $[Pep + M]^{2+}$ ISPs with $[Pep + H]^{+}$ ISPs shows the ability of the alkaline-earth cation to interact with some polar aliphatic residues (specifically Asp, Ser, and Thr, as well as the aromatic residues with Ba^{2+}). Comparisons of the relative difference of ISPs for alkaline-earth-coordinated to alkali-coordinated peptide ions show a lessened interaction of alkaline-earth cations with specific residues. This suggests general solvation by the peptide backbone within M^{2+}-coordinated systems. The interactions of these metals (alkali and alkaline-earth) with specific amino acid residues described by the ISP analysis are largely in agreement with the normalized frequencies of interaction reported from metalloprotein crystallographic data [53].

The ability of the ISPs to predict cross section is demonstrated by applying the $[Pep + M]^{2+}$ and $[Pep + 2H]^{2+}$ ISPs on the $[Pep + M + H]^{3+}$ dataset. Here we assume that the interactions that govern structure for $[Pep + M]^{2+}$ and $[Pep + 2H]^{2+}$ species can predict conformers that arise in the $[Pep + M + H]^{3+}$ species. These derived ISPs predict reduced cross sections within ±2 % to an observed feature within ~73 %, ~66 %, and ~74 % of the $[Pep + M + H]^{3+}$ peptides for Mg^{2+}, Ca^{2+}, and Ba^{2+}, respectively. Confomers predicted with the $[Pep + 2H]^{2+}$ ISPs are relatively more elongated, whereas the $[Pep + M]^{2+}$ ISPs generally predicted more compact conformers.

Acknowledgments

The authors are grateful for the software programming support used in data analysis provided by Michael A. Ewing. J.M.D. gratefully acknowledges the financial support received from the Ph.D. Fellowship provided by Naval Surface Warfare Center, Crane Division. Financial support was provided partially from the "Next Generation Threat" fund from Naval Surface Warfare Center, Crane Division (contract number N00164-08-C-JQ11) as well as from the METACyt Grant from the Lilly Endowment.

References

1. Sigel, H., Martin, R.B.: Coordinating properties of the amide bond. Stability and structure of metal ion complexes of peptides and related ligands. *Chem. Rev.* **82**, 385–426 (1982)
2. Holm, R.H., Kennepohl, P., Solomon, E.I.: Structural and functional aspects of metal sites in biology. *Chem. Rev.* **96**, 2239–2314 (1996)
3. Permyakov, E.A.: Metalloproteomics. Wiley, NJ, p. 1–36 (2009)
4. Wattenberg, A., Sobott, F., Barth, H.-D., Brutschy, B.: Studying noncovalent protein complexes in aqueous solution with laser desorption mass spectrometry. *Int. J. Mass Spectrom.* **203**, 49–57 (2000)
5. Kohtani, M., Kinnear, B.S., Jarrold, M.F.: Metal-ion enhanced helicity in the gas phase. *J. Am. Chem. Soc.* **122**, 12377–12378 (2000)
6. Taraska, J.A., Counterman, A.E., Clemmer, D.E.: Large anhydrous polyalanine ions: Substitution of Na^{+} for H^{+} destabilizes folded states. *Int. J. Mass Spectrom.* **204**, 87–100 (2001)
7. Nousiainen, M., Derrick, P.J., Kaartinen, M.T., Mäenpää, P.H., Rouvinen, J., Vainiotalo, P.: A mass spectrometric study of metal binding to osteocalcin. *Chem. Biol.* **9**, 195–202 (2002)
8. Chitta, R.K., Gross, M.L.: Electrospray ionization-mass spectrometry and tandem mass spectrometry reveal self-association and metal-ion binding of hydrophobic peptides: A study of the gramicidin dimer. *Biophys. J.* **86**, 473–479 (2004)
9. Ruotolo, B.T., Tate, C.C., Russell, D.H.: Ion mobility-mass spectrometry applied to cyclic peptide analysis: conformational preferences of gramicidin S and linear analogs in the gas phase. *J. Am. Soc. Mass Spectrom.* **15**, 870–878 (2004)
10. Ruotolo, B.T., Russell, D.H.: Gas-phase conformations of proteolytically derived protein fragments: Influence of solvent on peptide conformation. *J. Phys. Chem. B* **108**, 15321–15331 (2004)
11. Kohtani, M., Jarrold, M.F., Wee, S., O'Hair, R.A.J.: Metal ion interactions with polyalanine peptides. *J. Phys. Chem. B* **108**, 6093–6097 (2004)
12. Liu, D., Seuthe, A.B., Ehrler, O.T., Zhang, X., Wyttenbach, T., Hsu, J.F., Bowers, M.T.: Oxytocin-receptor binding: Why divalent metals are essential. *J. Am. Chem. Soc.* **127**, 2024–2025 (2005)
13. Lepšík, M., Field, M.J.: Binding of calcium and other metal ions to the EF-hand loops of calmodulin studied by quantum chemical calculations and molecular dynamics simulations. *J. Phys. Chem. B* **111**, 10012–10022 (2007)
14. Wyttenbach, T., Liu, D., Bowers, M.T.: Interactions of the hormone oxytocin with divalent metal ions. *J. Am. Chem. Soc.* **130**, 5993–6000 (2008)
15. Faull, P.A., Korkeila, K.E., Kalapothakis, J.M., Gray, A., McCullough, B.J., Barran, P.E.: Gas-phase metalloprotein complexes interrogated by ion mobility-mass spectrometry. *Int. J. Mass Spectrom.* **283**, 140–148 (2009)
16. Pan, J., Konermann, L.: Calcium-induced structural transitions of the calmodulin-melittin system studied by electrospray mass spectrometry:

Conformational subpopulations and metal-unsaturated intermediates. *Biochemistry* **49**, 3477–3486 (2010)
17. Murariu, M., Dragan, E.S., Drochioiu, G.: Electrospray ionization mass spectrometric approach of conformationally-induced metal binding to oligopeptides. *Eur. J. Mass Spectrom.* **16**, 511–521 (2010)
18. Wyttenbach, T., Grabenauer, M., Thalassinos, K., Scrivens, J.H., Bowers, M.T.: The effect of calcium ions and peptide ligands on the relative stabilities of the calmodulin dumbbell and compact structures. *J. Phys. Chem. B* **114**, 437–447 (2010)
19. Berezovskaya, Y., Armstrong, C.T., Boyle, A.L., Porrini, M., Woolfson, D.N., Barran, P.E.: Metal binding to a zinc-finger peptide: A comparison between solution and the gas phase. *Chem. Commun.* **47**, 412–414 (2011)
20. Chen, L., Gao, Y.Q., Russell, D.H.: How alkali metal ion binding alters the conformation preferences of gramicidin A: A molecular dynamics and ion mobility study. *J. Phys. Chem. A* **116**, 689–696 (2012)
21. Dunbar, R.C., Steill, J.D., Polfer, N.C., Oomens, J.: Peptide length, steric effects and ion solvation govern zwitterion stabilization in barium-chelated di- and tripeptides. *J. Phys. Chem. B* **113**, 10552–10554 (2009)
22. Dunbar, R.C., Steill, J.D., Oomens, J.: Conformations and vibrational spectroscopy of metal-ion/polyalanine complexes. *Int. J. Mass Spectrom.* **297**, 107–115 (2010)
23. Dunbar, R.C., Steill, J.D., Oomens, J.: Encapsulation of metal cations by the PhePhe ligand: A cation-pi ion cage. *J. Am. Chem. Soc.* **133**, 9376–9386 (2011)
24. Dunbar, R.C., Steill, J.D., Polfer, N.C., Berden, G., Oomens, J.: Peptide bond tautomerization induced by divalent metal ions: Characterization of the iminol configuration. *Angew. Chem. Int. Ed.* **51**, 4591–4593 (2012)
25. Fenn, J.B., Mann, M., Meng, C.K., Wong, S.F., Whitehouse, C.M.: Electrospray ionization for mass spectrometry of large biomolecules. *Science* **246**, 64–71 (1989)
26. Reiter, A., Zhao, H., Adams, J.: Intrinsic specificity of Ca^{2+}-protein binding sites. *Org. Mass Spectrom.* **1993**(28), 1596–1601 (1993)
27. Hu, P., Sorensen, C., Gross, M.L.: Influences of peptide side chains on the metal ion binding site in metal ion-cationized peptides: Participation of aromatic rings in metal chelation. *J. Am. Soc. Mass Spectrom.* **6**, 1079–1085 (1995)
28. Gross, D.S., Williams, E.R.: Structure of gramicidin S $(M + H + X)^{2+}$ ions (X = Li, Na, K) probed by proton transfer reactions. *J. Am. Chem. Soc.* **118**, 202–204 (1996)
29. Loo, J.A., Hu, P.: Interaction of angiotensin peptides and zinc metal ions probed by electrospray ionization mass spectrometry. *J. Am. Soc. Mass Spectrom.* **1994**(5), 959–965 (1994)
30. Nemirovskiy, O.V., Gross, M.L.: Determination of calcium binding sites in gas-phase small peptides by tandem mass spectrometry. *J. Am. Soc. Mass Spectrom.* **1998**(9), 1020–1028 (1998)
31. Sudhir, P.-R., Wu, H.-R., Zhou, Z.-C.: An application of electrospray ionization tandem mass spectrometry to probe the interaction of Ca^{2+}/Mg^{2+}/Zn^{2+} and Cl^- with gramicin A. *Rapid Commun. Mass Spectrom.* **19**, 1517–1521 (2005)
32. Dilger, J.M., Valentine, S.J., Glover, M.S., Clemmer, D.E.: A database of alkali metal-containing peptide cross sections: Influence of metals on size parameters for specific amino acids. *Int. J. Mass Spectrom.* **330–332**, 35–45 (2012).
33. Valentine, S.J., Ewing, M.A., Dilger, J.M., Glover, M.S., Geromanos, S., Hughes, C., Clemmer, D.E.: Using ion mobility data to improve peptide identification: Intrinsic amino acid size parameters. *J. Proteome Res.* **10**, 2318–2329 (2011)
34. Valentine, S.J., Counterman, A.E., Clemmer, D.E.: A database of 660 peptide ion cross sections: Use of intrinsic size parameters for bona fide predictions of cross sections. *J. Am. Soc. Mass Spectrom.* **10**, 1188–1211 (1999)
35. Henderson, S.C., Li, J., Counterman, A.E., Clemmer, D.E.: Intrinsic size parameters for Val, Ile, Leu, Gln, Thr, Phe, and Trp residues from ion mobility measurements of polyamino acid ions. *J. Phys. Chem. B* **103**, 8780–8785 (1999)
36. Valentine, S.J., Counterman, A.E., Hoaglund-Hyzer, C.S., Clemmer, D.E.: Intrinsic amino acid size parameters from a series of 113 lysine-terminated tryptic digest peptide ions. *J. Phys. Chem. B* **103**, 1203–1207 (1999)
37. Cargile, B.J., Bundy, J.L., Stephenson Jr., J.L.: Potential for false positive identifications from large databases through tandem mass spectrometry. *J. Proteome. Res.* **3**, 1082–1085 (2004)
38. Revercomb, H.E., Mason, E.A.: Theory of plasma chromatography/gaseous electrophoresis: A review. *Anal. Chem.* **47**, 970–983 (1975)
39. Mason, E.A., McDaniel, E.W.: Transport Properties of Ions in Gases. Wiley, New York (1988)
40. St. Louis, R.H., Hill, H.H.: Ion mobility spectrometry in analytical chemistry. *Crit. Rev. Anal. Chem.* **21**, 321–355 (1990)
41. Hoaglund-Hyzer, C.S., Counterman, A.E., Clemmer, D.E.: Anhydrous protein ions. *Chem. Rev.* **99**, 3037–3079 (1999)
42. Wyttenbach, T., von Helden, G., Batka, J.J., Carlat, D., Bowers, M.T.: Effect of the long-range potential on ion mobility measurements. *J. Am. Soc. Mass Spectrom.* **8**, 275–282 (1997)
43. Shvartsburg, A.A., Jarrold, M.F.: An exact hard spheres scattering model for the mobilities of polyatomic ions. *Chem. Phys. Lett.* **261**, 86–91
44. Mesleh, M.F., Hunter, J.M., Shvartsburg, A.A., Schatz, G.C., Jarrold, M.F.: Structural information from ion mobility measurements: Effects of the long range potential. *J. Phys. Chem.* **100**, 16082–16086 (1996)
45. Koeniger, S.L., Merenbloom, S.I., Clemmer, D.E.: Evidence for many resolvable structures within conformation types of electrosprayed ubiquitin ions. *J. Phys. Chem B* **110**, 7017–7021 (2006)
46. Koeniger, S.L., Merenbloom, S.I., Valentine, S.J., Jarrold, M.F., Udseth, H.R., Smith, R.D., Clemmer, D.E.: An IMS-IMS analogue of MS-MS. *Anal. Chem.* **78**, 4161–4174 (2006)
47. Merenbloom, S.I., Koeniger, S.L., Valentine, S.J., Plasencia, M.D., Clemmer, D.E.: IMS-IMS and IMS-IMS-IMS/MS for separating peptide and protein fragment ions. *Anal. Chem.* **78**, 2802–2809
48. Shaffer, S.A., Tang, K.Q., Anderson, G.A., Prior, D.C., Udseth, H.R., Smith, R.D.: A novel ion funnel for focusing ions at elevated pressure using electrospray ionization mass spectrometry. *Rapid Commun. Mass Spectrom.* **11**, 181–1817 (1997)
49. Shaffer, S.A., Prior, D.C., Anderson, G.A., Udseth, H.R., Smith, R.D.: An ion funnel interface for improved ion focusing and sensitivity using electrospray ionization mass spectrometry. *Anal. Chem.* **70**, 4111–4119 (1998)
50. Hoaglund, C.S., Valentine, S.J., Sporleder, C.R., Reilly, J.P., Clemmer, D.E.: Three-dimensional ion mobility/TOFMS analysis of electrosprayed biomolecules. *Anal. Chem.* **70**, 2236–2242 (1998)
51. ExPASy Proteomics Server PeptideMass: available at: http://expasy.org/tools/peptide-mass.html. Accessed 27 Aug 2010
52. Koeniger, S.L., Merenbloom, S.I., Sevugarajan, S., Clemmer, D.E.: Transfer of structural elements from compact to extended states in unsolvated ubiquitin. *J. Am. Chem. Soc.* **128**, 11713–11719 (2006)
53. Zheng, H., Chruszcz, M., Lasota, P., Lebioda, L., Minor, W.: Data mining of metal ion environments present in protein structures. *J. Inorg. Biochem.* **102**, 1765–1776 (2008)
54. Harding, M.M., Nowicki, M.W., Walkinshaw, M.D.: Metals in protein structures: A review of their principal features. *Crystallogr. Rev.* **16**, 247–302 (2010)
55. Shannon, R.D.: Revised effective ionic radii and systematic studies of interatomic distances in halides and chalcogenides. *Acta Crystallogr. A* **32**, 751–767 (1976)
56. Leon, S.J.: Linear Algebra with Applications, 3rd edn. Macmillan, New York (1990)
57. Dunbar, R.C., Polfer, N.C., Berden, G., Oomens, J.: Metal ion binding to peptides: Oxygen or nitrogen sites? *Int. J. Mass Spectrom.* **330–332**, 71–77 (2012)